International Journal of Nanoelectronics and Materials
Volume 11, No. 2, Apr 2018 [211-220]

Vertical-Cavity Surface-Emitting Lasers for Ultra-High Speed Photonics

Moustafa Ahmed[1*], Hameeda R. Ibrahim[1,2] and Fumio Koyama[2]

[1]Department of Physics, Faculty of Science, Minia University, 61519 Minia, Egypt.
[2]Precision & Intelligence Laboratory, Tokyo Institute of Technology, Japan.

Received 27 September 2017; Revised 24 October 2017; Accepted 6 December 2017

ABSTRACT

We propose a vertical-cavity surface-emitting laser (VCSEL) with a transverse-coupled-cavity (TCC) for a larger enhancement of the modulation bandwidth used in ultra-high-speed photonics. The dynamics of the TCC-VCSEL were analyzed over three characteristic regimes of OFB that correspond to continuous wave (CW) operation, pulsation, and chaos, depending on the coupling ratio between the VCSEL and feedback cavities. The intensity noise was evaluated in terms of the frequency spectrum of the relative intensity noise (RIN) and the carrier to noise ratio (CNR). The results show that strong lateral OFB can boost the modulation bandwidth to frequencies approaching 70 GHz. The free-running TCC-VCSEL follows CW operation, pulsation, and then chaos with the increase of coupling ratio. Under weak OFB, RIN is lowest under CW operation, increases under pulsing, and is pronounced in the chaos region. A TCC VCSEL with a short feedback cavity shows a stable CW operation without noticeable change in either RIN or CNR.

Keywords: Surface Emitting Laser, Ultra High Speed Photonics, TCC-VCSEL, Transverse-Coupled-Cavity, Modulation Bandwidth.

1. INTRODUCTION

VCSELs have small size, are low cost, have high-speed operation, have low power consumption, and can be fabricated into arrays [1,2]. These advantages cause VCSELs to attract much attention for use in photonics, e.g. fiber communications, radio-over fiber networks, optical data centers. Because the modern versions of these applications require dense traffic and high-speed transmission, the development of high speed VCSELs is a key issue. Various approaches have been reported to increase the speed of VCSELs. Subjecting the semiconductor laser to external OFB is an efficient technique to enhance modulation bandwidth. OFB has been used for increasing the bandwidth frequency of VCSELs [3,4], linewidth narrowing [5,6], decreasing the frequency chirp [7], and the stability of mode operation [8]. 60% improvement in modulation bandwidth was expected by Dalir and Koyama using TCC feedback [9,10]. Ahmed et al. [11] analyzed the modulation characteristics of TCC VCSELs and explained the bandwidth improvement as a type of photon-photon resonance.

Lang and Kobgyashi [12] incorporated the OFB effect in the rate equation model of semiconductor laser by adding a time-delay feedback term. This model is used only for weak and intermediate value of OFB and it is commonly followed by theoretical groups. Abdulrhmann *et al*. [13] improved the time-delay model of Lang-Kobgyashi to analyze and

*Corresponding Author: *mostafa.farghal@mu.edu.eg*

classify laser operation and dynamics under strong OFB. On the other hand, operation stability and noise of the laser is an important issue for applications. Despite the advantages of applying OFB in VCSEL, OFB may change CW operation dynamic to dynamics in the form of periodic oscillation, period doubling, quasi-periodicity, and even chaos [14], depending on the intensity and phase of the OFB radiation. These instabilities deteriorate the noise performance of the device [15]. Analysis of noise in VCSELs under OFB is then necessary for developing high-speed VCSELs with high performance for application in high-speed photonics.

In this work, we present the modeling of TCC VCSELs, demonstrating how strong lateral optical feedback can enhance the modulation bandwidth to record 70 GHz. OFB was treated as time delay of the electric field of the slow light in the TCC with multiple round trips. Also, we present computer simulation of the intensity noise in these VCSELs, and report on a design for low noise operation. The intensity noise was determined according to RIN and CNR.

2. THEORETICAL MODEL

The proposed TCC-VCSEL is sketched in Figure 1. The VCSEL is integrated with an external cavity out of a bow-tie oxide aperture [9]. In the lateral direction, light slows down and move in a zigzag fashion inside the VCSEL cavity with angle $\Phi \sim 90^0$ in the TCC. In the TCC of length L_C, the slow light is totally reflected back inside the VCSEL cavity. The lateral light travels in the TCC with a round trip time of $\tau = 2n_g L_C / c$, where $n_g = fn$ is group velocity, n is average material refractive index, and f is the slowdown factor of light inside TCC. After each round trip, the laser light is injected into the VCSEL cavity with a coupling ratio η. OFB is treated as the time delay of the electric field of the slow light in the TTC with multiple round trips. The present model of lateral OFB in the TCC VCSEL is treated by using a time-delay rate equation model of edge-emitting lasers under strong OFB in [13].

The time-delay rate equation model is presented according to the following rate equations of the carrier number *N(t)* injected inside the active region, emitted photon number *S(t)*, and optical phase θ(t),

$$\frac{dN}{dt} = \frac{\eta_i}{e} I(t) - \frac{N}{\tau_s} - \Gamma G S + f_N(t) \tag{1}$$

$$\frac{dS}{dt} = \left[\Gamma G - \frac{1}{\tau_p} + \frac{v_g}{W} \ln|U| \right] S + \Gamma R_{sp} + f_S(t) \tag{2}$$

$$\frac{d\theta}{dt} = \frac{1}{2}\left(\alpha\Gamma \frac{a}{V}(N - N_{th}) - \frac{c}{n_g W}\varphi \right) + f_\theta(t) \tag{3}$$

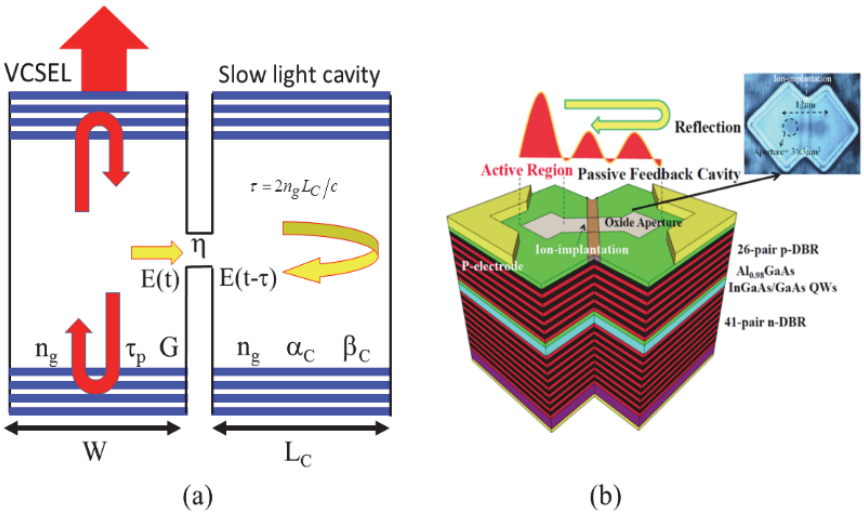

Figure 1. Scheme of VCSEL with TCC: (a) theoretical model and (b) structure.

In the above equations, Γ is the confinement factor, V volume of the active region, G optical gain, a differential gain, R_{sp} rate of spontaneous emission. N_T transparency electron number, η_i the injection efficiency, ε gain suppression coefficient, τ_p photon lifetime, τ_s electron lifetime due to spontaneous emission, and N_{th} electron number at threshold. The lateral OFB is included in the time-delay function $U(t-\tau)$ as

$$U = 1 + \frac{\eta}{1-\eta} \sum_k \sqrt{1-\eta}^{k} \, e^{-2k\alpha_C L_C} e^{-j2k\beta_C L_C} \sqrt{\frac{S(t-k\tau)}{S(t)}} e^{j\theta(t-k\tau)-j\theta(t)} \tag{4}$$

where $\theta(t)-\theta(t-k\tau)$ is the deflection in the optical phase in round trip k due to frequency chirp, while the terms $\exp(-2k\alpha_C L_C)$ and $\exp(-2kj\beta_C L_C)$ represent the loss and phase delay suffered by the slow light in round trip m, respectively. $\alpha_C = f\alpha_m$ and $\beta_C = 2\pi n/(\lambda f)$ are the optical loss and propagation constant, respectively.

The direct current modulation of the device is described as

$$I(t) = I_b + I_m \sin(2\pi f_m t) \ , \tag{5}$$

where I_b is the DC current and I_m is the modulation current. The modulation depth is defined as $m = I_m / I_b$. Finally, $F_N(t)$, $F_S(t)$ and $F_\theta(t)$ in equations (1) – (3), respectively, are given by [16]

$$f_s(t) = \sqrt{\frac{2R_{sp}\Gamma S(t)}{\Delta t}}.x_S \tag{6}$$

$$f_N(t) = \sqrt{\frac{2N(t)}{\tau_S \Delta t}}.x_n - \sqrt{\frac{2R_{sp}S(t)}{\Delta t}}.x_S \tag{7}$$

And $$f_\theta = \sqrt{\frac{R_{sp}\ \Gamma}{2\,S(t)\,\Delta t}}.x_\theta$$

where x_s, x_n and x_θ are three independent random numbers with Gaussian probability distributions.

The frequency content of intensity fluctuations is measured in terms of RIN, which is calculated as the Fourier transformation of the photon number fluctuations $\delta S(t) = S(t) - S_b$ around the bias value S_b. Over a finite time T, RIN is given as [16]

$$RIN = \frac{1}{S_b^2}\left\{\frac{1}{T}\left|\int_0^T \delta S(t) e^{-j2\pi f\tau} d\tau\right|^2\right\} \tag{8}$$

For LF-RIN, we take the average values of the RIN components over frequencies lower than 100 kHz.

2. PROCEDURES OF NUMERICAL CALCULATIONS

To explain the modulation bandwidth enhancement and dynamics of TCC-VCSEL, we used the fourth-order Runge-Kutta method to solve the rate equations numerically. Also, we plotted the bifurcation diagram to study the effect of the mount of OFB on VCSEL dynamics. The time step was taken as 2ps for high accuracy. We used multiple round trips in our calculations with k_{max} = 6 rounds. First, we solved the integration without OFB, i.e., with time between 0 and τ. The values of $S(t=0\rightarrow\tau)$ and $\theta(t=0\rightarrow\tau)$ were then stored for use as values of time-delays $S(t\rightarrow\tau)$ and $\theta(t\rightarrow\tau)$ for the integration of rate equations over the period $t=(t\rightarrow 2\tau)$ with OFB terms and so on for all round trips. The total calculation time should be higher than 1.1 μs to reach the stable operation of laser [14]. The numerical values of the laser parameters used in the calculations are listed in table 1.

Table 1 VCSEL parameters and their numerical values [17]

Parameter	Value
Active region refractive index of n	3.3
Material loss of active region α_m	10 cm^{-1}
Slow down factor f	50
Volume of active region V	1.76×10^{-19} m^3
Width of active region W	4 μm
Differential gain a	3.64×10^{-12} m^3s^{-1}
Confinement factor Γ	0.0382
Electron number at transparency N_T	3.17×10^5
Gain suppression coefficient ε	1.5×10^{-5} s^{-1}
Lifetime of photon τ_p	2 ps
Spontaneous emission factor R_{sp}'	1.16×10^{10} s^{-1}
Efficiency of injection η_i	0.8
Electron lifetime τ_s	1.5 ns
Linewidth enhancement factor α	2

3. RESULTS AND DISCUSSION

3.1 Improving Modulation Bandwidth

We present in Figure 2 the results on the bandwidth enhancement of VCSEL induced by coupling it with TCC. The figure plots the IM response whenthe modulation index is m=0.01 under different values of coupling ratioη when L_C = 20 μm. The figure shows that the IM response of the VCSEL without feedback has a peak at the carrier-photon resonance (CPR)frequency of 12 GHz, and bandwidth frequency off_{3dB0}= 24 GHz. The plotted examples of the IM responses have improved modulation characteristics over that of the conventional VCSEL. The modulation bandwidth improves to f_{3dB} = 33.5 GHz when $\eta = 0.5$, due to shifts in CPR frequency to a higher frequency of f_m = 16 GHz and as CPR peak reaches ~ 5 dB. When the coupling ratio increase to $\eta = 0.7$, f_{3dB}increases further to 42 GHz; that is, f_{3dB}79 higher than that of the conventional VCSEL. This result is much larger than the percentage of 60% reported in [10]. The IM response does not drops below the –3dB level; but we can see another peak of value ~ 1.4 dB at the mm-wave frequency of f_m = 39 GHz. Under very strong OFB of η = 0.96, the figure indicates further improvement of the IM-response; the mm-wave peak shifts to a frequency of 49.6 GHz, which is much higher than that of the CPR peak. This IM response can be considered as a type of extended CPR to the mm-wave region [11].

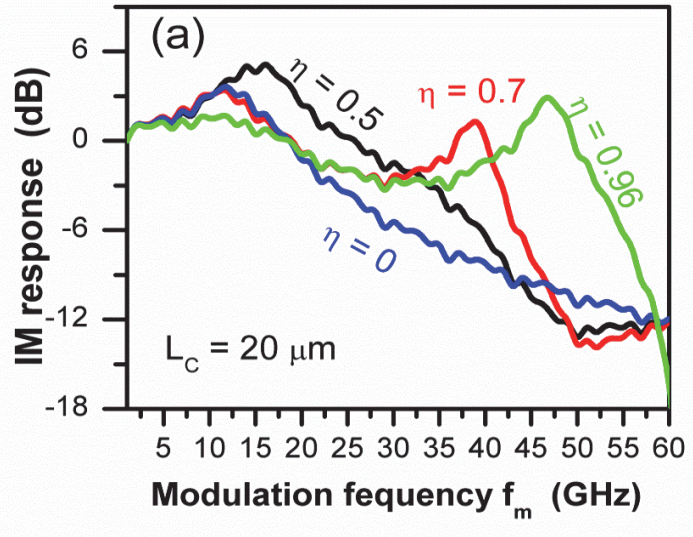

Figure 2. Frequency spectrum of the IM responses under different values of η: with CPR.

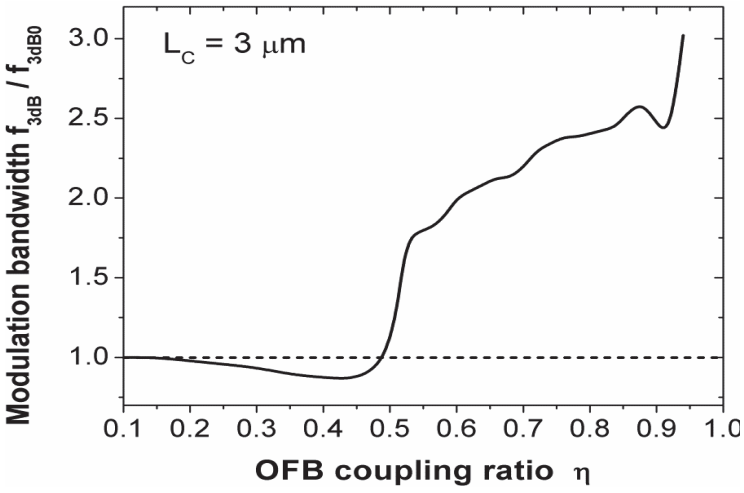

Figure 3. The modulation bandwidth frequency f_{3dB} as a function of the coupling ratio η when the TCC length is L_C = 3 μm.

Figure 3 plots the relation between the coupling coefficient η and the modulation bandwidth f_{3dB} when the length of TCC is $L_C = 3$ μm. When the coupling ratio $\eta = 0.45$, the figure indicates that the f_{3dB} is drops to 0.87 f_{3dB0} with the increase in the OFB strength. When the coupling ratio increases further, the figure shows large enhancement in f_{3dB}, indicating that the strong OFB has a large effect to inducing high-modulation bandwidth frequencies. When $\eta = 0.94$ the modulation bandwidth f_{3dB} is further enhanced, up to $3f_{3dB0}$.

3.2 Dynamics and Analysis of Noise in TCC-VCSEL

Before presenting the results on the noise subject, we explain the characteristics of the TCC VCSEL dynamics under OFB, and show the induced dynamics classes. For this purpose, we use the bifurcation diagram of the laser intensity. The bifurcation diagram was constructed at a fixed injection current by sampling the peaks S_{peak} of the time-varying photon number and plotting these peaks (normalized by the bias value S_b) as a function of the coupling ratio η. Figure 4 plots this bifurcation diagrams when the length of TCC is L_C = 15μm. The figure indicates that the operation of the TCC-VCSEL is stable CW when the OFB is as weak as η <0.35. The dynamics of the CW operation are presented in the figure as single circuits at S_{peak}/S_b=1. Then, the VCSEL emits periodic oscillations starting from η=0.34. Many closely spaced points at each η in the figure represent this pulsation. For intermediate values of η, more than two oscillation periods are induced, attracting the VCSEL to the chaotic region. With the increase in η, the VCSEL there after catches again to a stable CW operation when η > 0.63.

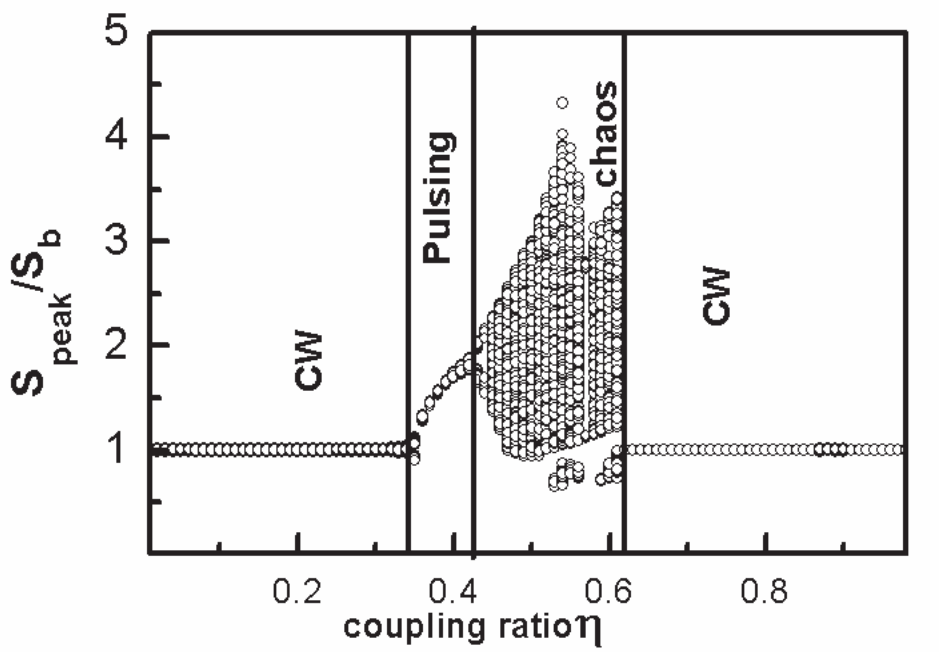

Figure 4. Bifurcation diagram of $S(t)$ with η when L_C=15μm.

3.3 Characteristics of TCC-VCSELs Dynamic States

Typical signal shapes of the TCC-VCSEL dynamic types and frequency spectra of RIN (dB/Hz) are shown in figures 5(a) – (d) and 6(a) – (d), respectively. These figures correspond to η= 0.2 (weak OFB), $\eta = 0.4$ (intermediate OFB), $\eta = 0.54$ (rather intermediate OFB), and $\eta = 0.9$ (strong OFB). Figure 5(a) characterizes the weak regime of OFB with CW operation, and shows that the emitted photon number *S(t)* is almost coincident with that of the conventional VCSEL. Figure 5(b) corresponds to the rather intermediate value of the coupling ratio η = 0.4 and

characterizes the periodic oscillation; *S(t)* oscillates with a period close to $1/f_r$ where f_r is the CPR frequency of the VCSEL. In this dynamic type, OFB is strong enough to make the relaxation oscillation undamped and then generate pulses. Figure 5(c) plots the extremely unstable dynamic state of chaos in the intermediate range of OFB (η =0.54). This state is characterized by an irregular variation of *S(t)* with time variation. These characteristics are in agreement with those obtained by Ahmed *et al*. in [11,18]. Under very strong OFB with η = 0.9, Figure. 5(d) shows that the CW operation is re-generated. The characteristics of this CW operation are almost coincident with those of the conventional VCSEL. These characteristics are in agreement with the expectations of Ahmed *et al.* [18]

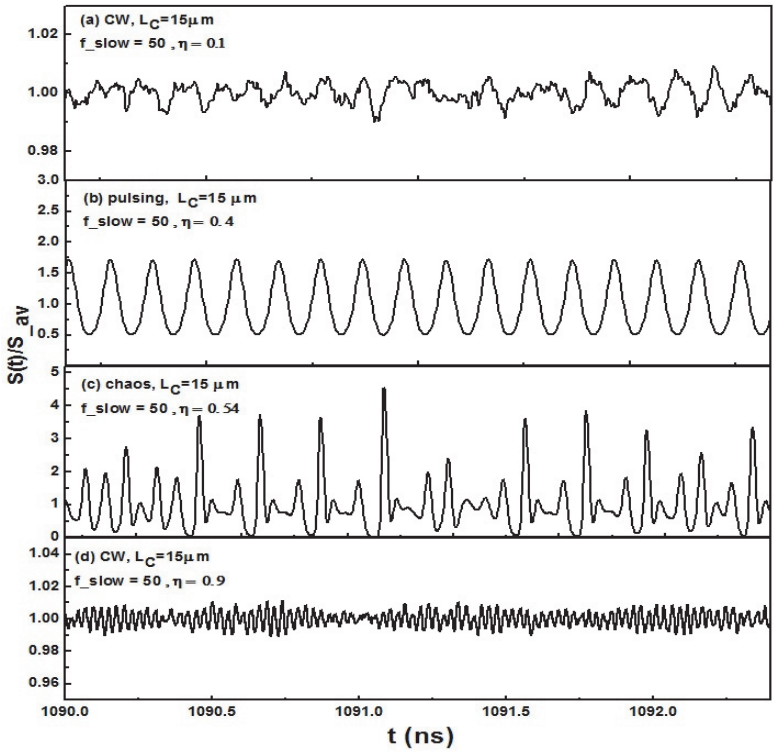

Figure 5. Signal characteristics of (a) CW (η =0.2), (b) pulsing (η = 0.4), (c) chaos (η = 0.54), and (d) CW (η =0.9) when L_C=15μm.

Figures 6(a) – (d) show the frequency spectra of RIN that correspond to the signal shapes in Figure 5(a) – (d) respectively. The RIN spectrum of the VCSEL without OFB is also presented in the figures plotted with dashed line for comparison. Figure 6(a) corresponds to the CW operation, which characterizes the weak regime of coupling ratio η= 0.1. The RIN spectrum presented in this figure is comparable to that of the conventional VCSEL, exhibiting the pronounced peak around the CPR frequency. It implies that the weak value of the coupling ratio is not sufficient to change the relaxation oscillation frequency of TCC-VCSEL. Figure 6(b) corresponds to the intermediate value of the coupling ratio η= 0.4, which is characterized by period-1 oscillations. The RIN spectrum has a very sharp peak around a frequency comparable to the CPR frequency and other peaks at higher harmonics. These characteristics are in agreement with those reported by Ahmed *et al.* [19]. Figure 6(c) plots the RIN spectrum of the chaotic dynamics induced by OFB when η=0.54. The figure shows the noisiest chaotic state suffered by the VCSEL in the intermediate range of OFB. In this case, RIN is 40 dB higher than that of the VCSEL without OFB. Figure 6(d) shows the RIN spectrum characterizing the stable CW operation in the regime of strong OFB (η = 0.9). This RIN spectrum is almost the same as that of the CW operation of η= 0.1.

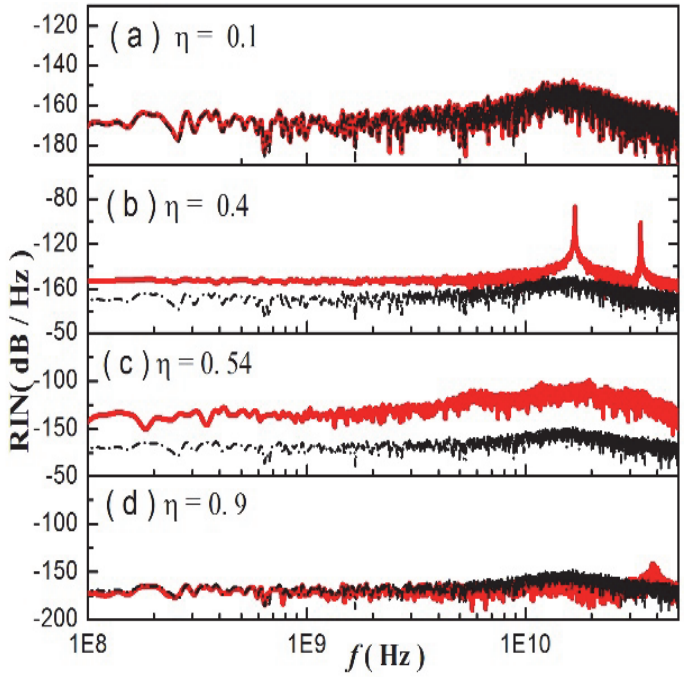

Figure 6. RIN spectrum of (a) CW (η=0.1), (b) pulsing (η=0.4), (c) chaos (η=0.54) and (d) CW (η=0.9) when L_C = 15μm. The RIN spectrum of the solitary VCSEL is plotted by the dashed line.

We investigate the variation of noise with the strength of OFB. The noise was calculated in terms of low-frequency RIN (LF-RIN) as well as CNR. The results are plotted in Figure 7, which plots CNR on the left-hand axis and LF-RIN on the right-hand axis as functions of coupling ratio η. The figure indicates that LF-RIN is lowest under the CW operation, and increases slowly under the period-1 oscillations. When η increases beyond 0.41, LF-RIN increases and is pronounced in the chaos region. When η> 0.63, LF-RIN drops to lower levels again under the CW operations. The figure also shows that under CW operation, CNR is almost in the same level as that of the VCSEL without OFB. CNR decreases with the increase in coupling ratio η under the period-1 oscillation and reaches the lowest values under the chaotic dynamics before restoring the upper limit of the strong OFB-induced CW operation.

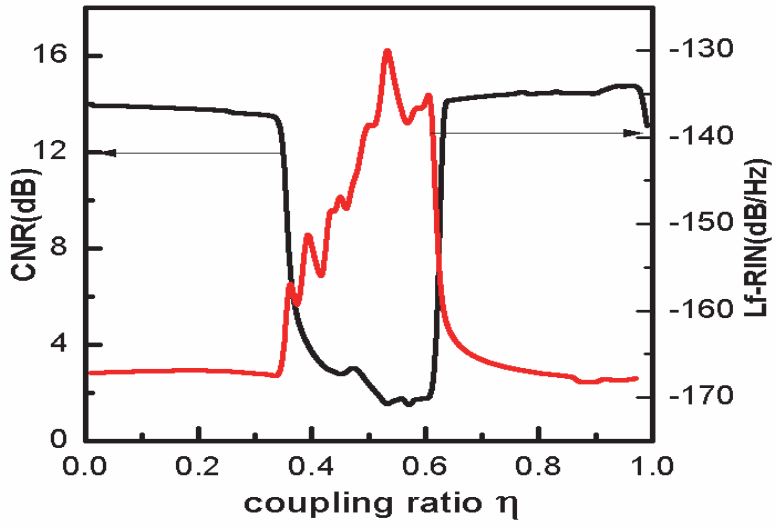

Figure 7. Variation of LF-RN and CNR with η when L_C=15μm.

3.4 Influence of TCC Length on Noise Performance of TCC VCSEL

In this subsection, we focus on finding out the optimum length of the TCC that corresponds to the best noise performance of TCC VCSEL. In figures 8(a) and (b), we plot both CNR and LF-RIN as functions of the length T_C of the TCC cavity respectively, under different strengths of OFB of η = 0.1, 0.4, and 0.9. The figure shows that regardless of the value of η, when the TCC cavity is shorter than L_C = 8 μm, both CNR and LF-RIN are comparable to those of the VCSEL without feedback; no noticeable excess noise is seen. In this case, the TCC VCSEL operates a under stable CW operation for different values of coupling ratios. The same situation applies to the length range of 10μm < L_C < 13μm. The shown enhanced values of LF-RIN and lowered values of CNR when η = 0.4 correspond to lengths that result in regular and/or irregular oscillations.

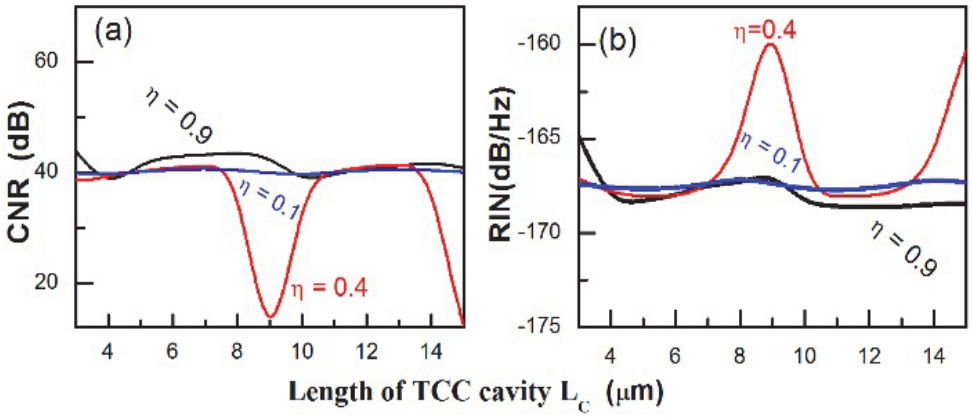

Figure 8. (a)Variation of (a) CNR and (b) LF-RIN with the TCC length L_C.

4. CONCLUSIONS

We presented the modeling and simulation of the dynamics and noise of VCSELs coupled to a transverse cavity, which is designed to operate at high speeds. The mechanism in which the TCC works to enhance the modulation bandwidth of TCC VCSEL was modeled and explained. The modulation bandwidth can increase beyond 70 GHz when the length of the TCC is 3 μm and the coupling ratio is as large as 0.96. The noise performance of the TCC VCSEL is optimized when the VCSEL operates in CW, which is dominant when the length of the transverse cavity is lower than 8 μm and over the range of 10μm < L_C < 13μm. When the TCC VCSEL emits regular and/or irregular oscillations, RIN is enhanced and CNR is lowered.

REFERENCES

[1] K. Iga. *Jpn. J. Appl. Phys.* **47**, 1R (2008) 1.
[2] F. Koyama, *J. Lightw. Technol.* **24**, 12 (2006) 4502.
[3] X. Zhao, D. Parekh, E. K. Lau, H.K. Sung, M. C. Wu, W. Hofmann, M. C. Amann, C. J. Chang-Hasnain, *Opt. Exp.* **15** 22 (2007) 14810.
[4] S. H. Lee, D. Parekh, T. Shindo, W. Yang, P. Guo, D. Takahashi, N. Nishiyama, C. J. Chang-Hasnain, S. Arai, *Opt. Exp.* **18** 16 (2010) 16370.
[5] J. Harrison, A. Mooradian, *IEEE J. Quantum Electron*. **25** (1989) 1152.
[6] J. M. Kahn, C. A. Burrus, G. Raybon, *IEEE Photon. Technol. Lett*. **1** (1989) 159.
[7] G. P. Agrawal, C. H. Henry, *IEEE J. Quantum Electron*. 24 (1988)134.
[8] G. Wenke, R. Gross, P. Meissner, E. Patzak, *J. Light wave Technol*. **5** (1987) 608.
[9] H. Dalir and F. Koyama, Appl. Phys. Lett. **103**, 9, (2013) 091109.
[10] H. Dalir and F. Koyamad, *IEICE Electron. Exp.* **8**,13 (2011) 1075.

[11] M. F. Ahmed, A. Bakry, R. Altuwirqi, M. S. Alghamdi, F. Koyama, *Jpn. J. Appl. Phys.* **52**, 12 (2013) 124103.
[12] R. Lang, K. Kobayashi, *IEEE J. Quantum Electron.,* QE-**16** (1980) 347.
[13] *S. Abdulrhmann, M .Ahmed, T. Okamoto, W. Ishimori, M. Yamada*, IEEE. J. Quantum. Electron. 9 (2003) 1265.
[14] S. Abdulrhmann, M. Ahmed, M. Yamada, *SPIE* 4986 (2003) 490.
[15] J. Mork, Ph.D. Thesis., Technical University of Denmark, Denmark (1988).
[16] K. I. Kallimani, M. J. O. Mahony, *IEEE J. Quantum Electron*. 34 (1998) 1438.
[17] L. A. Coldren, S. W. Corzine, M. L. Mashanovitch, 2nd ed. New York, NY: Wiley, (2012) 260.
[18] M. Ahmed, M. Yamada, S. W. Z. Mahmoud, *Int. J. Numer*. *Model*. **20** (2007) 117.
[19] M. Ahmed, N. Z. El-Sayed, H. Ibrahim, The European Physical Journal D 66, 5 (2012) 141.